Desalination and Water Treatment
www.deswater.com

doi: 10.5004/dwt.2019.23623

144 (2019) 300–310
March

Efficient removal of brilliant blue by clinoptilolite tuff modified with Fe^{3+} and Fe–Cu nanoparticles

S. Pinedo-Hernández[a], V. Sánchez-Mendieta[a,b], E. Gutiérrez-Segura[a], M. Solache-Ríos[c,*]

[a]*Universidad Autónoma del Estado de México, Facultad de Química. Paseo Colón esq. Paseo Tollocan, S/N. C.P. 50180, Toluca, México, emails: samantha_pinedo@yahoo.com.mx (S. Pinedo-Hernández), vsanchezm@uaemex.mx (V. Sánchez-Mendieta), eegutierrezs@uaemex.mx (E. Gutiérrez-Segura)*

[b]*Centro Conjunto de Investigación en Química Sustentable UAEM-UNAM, Carretera Toluca-Ixtlahuaca Km. 14.5, Tlachaloya, Toluca, Estado de México, México*

[c]*Instituto Nacional de Investigaciones Nucleares, Departamento de Química. Carretera México-Toluca S/N La Marquesa, C.P. 52750, Ocoyoacac, México, Tel. +52 5553297200 Ext. 2280; email: marcos.solache@inin.gob.mx*

Received 10 April 2018; Accepted 16 December 2018

ABSTRACT

Ferric-modified zeolitic tuff (Ze–Fe) and a composite of that modified zeolite bearing Fe–Cu nanoparticles (Ze–Fe(Fe–Cu)) were investigated for the removal of brilliant blue. The composite was synthesized by *in-situ* reduction of Fe and Cu salts using borohydride. Both materials were characterized by Brunauer–Emmett–Teller, X-ray diffraction, scanning electron microscopy, transmission electron microscopy (TEM), and infrared spectroscopy. TEM demonstrated that nanostructures of Fe–Cu (11.70–15.85 nm) were successfully dispersed on the zeolitic tuff. Batch experiments showed that the adsorption of dye is more favorable for Ze–Fe(Fe–Cu) than Ze–Fe; the kinetic adsorption data followed the second-order kinetic model. The results also showed that the removal of the dye was the highest between pH 3 and 5 for both materials. The removal of brilliant blue was 87.02% for Ze–Fe(Fe–Cu) and 75.29% for Ze–Fe. The $\Delta H°$ values of 52.60 kJ/mol for Ze–Fe and 126.29 kJ/mol for Ze–Fe(Fe–Cu) indicated that the adsorption processes are endothermic for both materials.

Keywords: Brilliant blue; Adsorption; Zeolite; Nanoparticles

1. Introduction

Dyes are one of the major groups of pollutants found in wastewaters, about 700,000 t of dyes are produced annually and about 20% is discharged from industry without a treatment. Azo, anthraquinone, sulfur, indigoid, triphenylmethane, and phthalocyanine are the dyes mostly used in the industry [1]. Studies on the treatments of wastewater-containing dyes have been an important area of research in recent years [2]. One important dye used in the industry is brilliant blue (Food blue No. 1, Erioglaucina, E133 (dye), C.I. Acid blue 9, CI Food blue 2, C.I.: 42090, molecular formula: $C_{37}H_{34}O_9N_2S_3Na_2$, wt.: 792.85 g/mol, pk_a: 5.83, 6.58) [3–6]; it is a weak acid organic molecule with polar and nonpolar components. Anionic molecules can bind to anion exchange sites of different adsorbents [7].

Dyes in natural water reduce light penetration which can modify the photosynthetic activity. Also, many dyes are toxic, carcinogenic, and mutagenic [8]. A wide range of methods have been developed to remove dyes from wastewaters, such as adsorption on organic or inorganic matrices, chemical precipitation, flocculation and coagulation, oxidation by chlorine, ozone electrolysis, electrochemical and microbiological treatments, etc. Some dyes are not completely removed from wastewater because most dyes are not amenable to common chemical, physical, or biological treatments due to their chemical stability, thus causing dangerous accumulation in the environment [9,10].

* Corresponding author.

Adsorption is one of the processes, which is widely used in wastewater treatments. Some of the main adsorbents used are silica gel, alumina, zeolites, activated carbon, sawdust, peat, lignite, and red mud [11]. Zeolites have shown to be efficient to remove dyes from water solutions [12]. They are useful to remove different pollutants because of their physicochemical properties [1]; clinoptilolite is one of the most abundant natural zeolite [13]. Zeolites contain exchangeable cations (Na^+, K^+, Ca^{2+}, Mg^{2+}, etc.), and these cations can be exchanged with organic and inorganic pollutants [14]. Modified zeolites and pillared clays have been used in discoloration of aqueous solutions and mineralization of dyes [8,9]. Zeolites can exchange cations including iron and copper; these cations are strongly attached to the zeolite networks, and they are not likely to leach out in aqueous solutions [15].

Nanoparticles of metals and metal oxides have been extensively used in many organic reactions because of their high surface area. Recently, several methods for the preparation of nanoparticles have been developed, such as thermal decomposition, coprecipitation from solution and laser pyrolysis, microwave plasma, electrochemical synthesis, sol–gel method, and mechanical activation by using microemulsion and other methods [16]. Iron nanoparticles are synthesized in the presence of supporting inorganic material [15,17–19].

Fe–Cu material is an useful adsorbent for the removal of organic matter from wastewater; Cu located on the iron surface (Fe/Cu particles) could accelerate the corrosion of Fe and the generation of [H^+] [20,21]. A few studies concerning the application of Cu-containing clinoptilolite have been reported [22].

In the present work, the brilliant blue adsorption behavior was evaluated with both an iron-modified zeolite tuff (Ze–Fe) and a composite (Ze–Fe(Fe–Cu)) considering contact time, initial dye concentration, and pH.

2. Materials and methods

2.1. Materials

The clinoptilolite-rich tuff was obtained from Villa de Reyes, State of San Luis Potosí, Mexico; it was milled and sieved. The grain size used was between 0.8 and 1.0 mm. The zeolitic (Ze) material was treated with a hydrochloric acid solution and shaked for 4 h (50 g of material with 500 mL of 0.5 M HCl solution). Afterward, the zeolitic material was washed with distilled water until no presence of chloride ions was observed in the washing solution tested with silver nitrate. The acid-treated zeolitic tuff (Ze–HCl) was then dried at room temperature. Ze–Fe was prepared by following the method reported elsewhere [23,24]; 47.5 g of zeolitic tuff (Ze–HCl) with 500 mL of 0.1 M $FeCl_3$ solution was refluxed for 5 h; this procedure was performed twice. The weight of the zeolitic material decreased after each conditioning; this behavior could be attributed to the removal of fine particles during the processes.

2.2. Preparation of Ze–Fe(Fe–Cu) composite

Composite of iron and copper nanoparticles supported on clinoptilolite was prepared by using the reduction method [25]; 5.34 g of $FeCl_3{\cdot}4H_2O$ was dissolved in 25.0 mL of ethanol/water (4:1) and mixed with 10 mL of a 0.2 M $Cu(NO_3)_2$ solution. Subsequently, 1.5 g of Ze–Fe was added to the solution and mixed with a magnetic stirrer for 15 min. $NaBH_4$ solution was prepared separately by dissolving 2.54 g in 70.0 mL of deionized water, and then it was added to the mixture under continuous stirring at a constant addition rate of 0.5 mL/s. After borohydride addition, the solution was kept under continuous stirring for 15 min and then filtered and washed 3 times with absolute ethanol. Finally, the material was dried in the oven at 90°C for 6 h. The nanoparticles N(Fe–Cu) were prepared without the addition of Ze–Fe.

2.2. Characterization

2.2.1. Scanning electron microscopy

The materials were mounted directly on the holders and then observed at 20 kV in a JEOL JSM-5900-LD electron microscope. The microanalysis was done with an energy X-ray dispersive spectroscopy (EDS) system.

2.2.2. X-ray diffraction

Powder diffractograms of the materials were obtained with a Bruker D8 Advance diffractometer coupled to a copper anode X-ray tube, operated with an accelerating voltage of 30 kV, with Bragg–Bretano chamber, and current emission of 25 mA. The conventional diffractograms were compared with the Joint Committee on Powder Diffraction Standards (JCPDS).

2.2.3. Infrared spectroscopy

The infrared (IR) spectra in the 4,000–500 cm^{-1} range were recorded at room temperature using an IR Prestige-21Shimadzu. Samples were prepared following the standard KBr pellet method.

2.2.4. Transmission electron microscopy

Ze–Fe(Fe–Cu) composite was suspended in 2-propanol using an ultrasonic instrument. TEM samples were prepared by placing a drop of the alcoholic suspension on carbon-coated copper grids. TEM observations were performed using a TEM JEOL-2010, operated at an accelerating voltage of 200 kV equipped with an LaB6 filament.

2.2.5. Specific surface areas (Brunauer–Emmett–Teller)

The Brunauer–Emmett–Teller (BET) specific surface areas were determined by standard multipoint techniques of nitrogen adsorption, using a Micromeritics Gemini 2360 instrument. The samples were heated at 373 K for 2 h before specific surface areas were measured.

2.2.6. Zero charge point

Aliquots (10 mL) of a 0.01 M NaCl solution were adjusted between pH 1 and 12 by adding 0.1 M HCl or NaOH solutions. Aliquots were left in contact with each adsorbent for 24 h, and then the samples were centrifuged and decanted,

and the pH was analyzed in the remaining liquid phases using a Hanna Instruments HI2550 Ph/ORP pH meter.

2.3. Adsorption kinetics

Kinetic removal of brilliant blue dye by the zeolitic tuff, acid-treated zeolitic tuff (Ze–HCl), Ze–Fe, and the composite Ze–Fe(Fe–Cu) was performed as follows: samples of 100 mg of each adsorbent and 10 mL aliquots of a 10 mg/L solution (pH 5.8) were placed in centrifuge tubes and shaken for different time intervals (5, 15, and 30 min, and 1, 3, 5, 7, 24, 48, and 72 h) at 120 rpm at 25°C. Later, the samples were centrifuged and decanted; the experiments were carried out in duplicate. The brilliant blue dye concentrations in the solutions were determined by using a UV/Vis Genesis 10S spectrophotometer analyzer, with λ = 630 nm. The pH of each solution was measured before and after the treatments.

2.4. Sorption isotherms

Samples of 100 mg of each adsorbent (Ze, Ze–HCl, Ze–Fe, and Ze–Fe(Fe–Cu) composite) were put in contact with 10 mL of different concentrations of brilliant blue dye solutions (10, 20, 40, 60, 80, 100, 120, 140, 160, and 180 mg/L) for 72 h at 25°C, and the samples were centrifuged and decanted. Dye concentrations were determined in the liquid phases as described above, and the pH was measured in each solution. The experiments were performed in duplicate.

Equilibrium sorption capacity was calculated using Eq. (1):

$$q_e = \frac{C_0 - C_e}{M} \times V \tag{1}$$

where q_e (mg/g) is the equilibrium sorption capacity, C_0 and C_e are the initial and equilibrium concentrations (mg/L) of brilliant blue, respectively, V (L) is the volume, and M (g) is the weight of the adsorbent.

The percent removal (%) of dye was calculated using the following equation:

$$\text{Removal}(\%) = \frac{C_0 - C_e}{C_0} \times 100 \tag{2}$$

2.5. Effect of pH

In order to check the effect of pH on brilliant blue uptake by the different sorbent materials, experiments were carried out by putting in contact 10 mL aliquots of a 10 mg/L solution of brilliant blue at different pH values (from 3 to 9) and 100 mg of each adsorbent. The pH values of the solutions were adjusted by adding 0.1 M HCl or NaOH solutions. The mixtures were shaken for 72 h and then centrifuged and decanted. The pH was measured in the remaining liquid phases using a Hanna Instruments HI2550 pH/ORP pH meter, and the dye concentrations were determined as above by UV/Vis spectrophotometry. The experiments were performed in duplicate.

3. Results and discussion

3.1. Characterization of the adsorbents

3.1.1 Scanning electron microscopy (SEM) and TEM

The morphology, particle size, and elemental analysis of Ze–Fe and Ze–Fe(Fe–Cu) were studied by SEM, and the corresponding SEM photographs are presented in Figs. 1(a)–(c). The crystallites of the zeolite have well-defined cubic shapes, which are characteristic morphologies of the clinoptilolite [26]. Fig. 1(d) shows the image of Ze–Fe(Fe–Cu). The Fe–Cu particles are distributed as agglomerates; the surface is relatively rough in comparison with the original sample. The EDS analysis was carried out in different areas for each adsorbent material (Ze, Ze–HCl, Ze–Fe, and Ze–Fe(Fe–Cu)). The main elements found in the adsorbent materials were O, Na, Mg, K, Ca, Fe, Al, Si (Table 1), Na^+, Mg^{2+}, K^+, and Ca^{2+} and are the extra framework cations that compensate the deficiency of negative charge in the zeolite network [27,28]. Ca, Na, and K concentrations decrease after treating the zeolitic tuff with $FeCl_3$. HCl treatment removes impurities; cations are exchanged by H^+ and dealuminate the zeolite structure [29]; in the experimental conditions of this work, dealumination was not observed. Na^+ and Ca^{2+} were replaced by H^+ or Fe^{3+} since the content of this last element was the highest in the zeolitic tuffs containing Fe [30]. It has been reported that the presence of iron in the zeolite may be located differently: as high-spin Fe^{3+} in framework tetrahedral sites, in extra framework octahedral sites as free $Fe(H_2O)_6^{3+}$, and as high-spin Fe^{2+} in octahedral coordination in extra framework sites or in another aluminosilicate sites associated with the zeolite. Iron is also found as magnetite component in the zeolite rocks [31]. Trgo and Perić [32] have shown that the amphoteric nature of hydroxyl surface groups (=(Al/Si)–OH) can lead to the formation of sites with different energies; this effect increases the number of possible adsorption locations. It can be observed that the elemental compositions determined by EDS before and after the adsorption experiments are similar. The composition persisted in the treated forms of clinoptilolite, confirming that the conditioning mainly affects the concentrations of exchangeable ions without causing significant alterations in the network of the zeolite; these findings are corroborated by the work done by Pinedo-Hernández et al. [33].

The morphology of the nanoparticles on the zeolite network was characterized by TEM. The TEM images (Figs. 1(g)–(i)) confirm that the dimensions of the Fe–Cu particles are in the nano regime, the size distribution shows particles that vary between 11.70 and 15.85 nm, and the TEM image reveals spherical particles as the main morphology. The presence of iron oxide and copper oxide is confirmed from the diffraction measurements (Fig. 3(b)); they indicate that the iron oxide particles were deposited on the surface of the zeolite matrix.

3.1.2. IR Spectroscopy

The IR spectra obtained from the samples of the natural zeolitic rock and the acidic zeolite rock were similar (Fig. 2), only slight changes in the percentage of transmittance were observed. The zeolite samples chemically treated with iron show no differences in the location of the vibrations with respect to the unmodified material. The absorption peaks

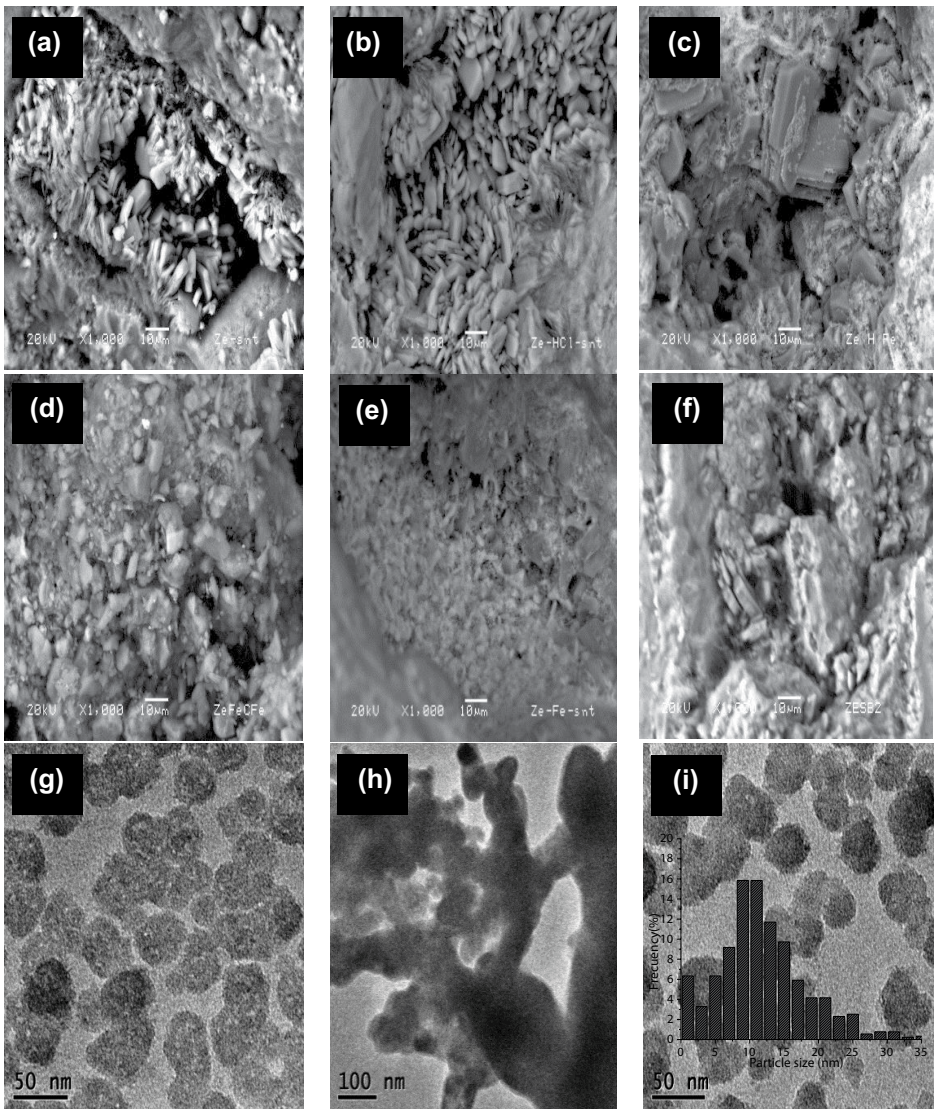

Fig. 1. Scanning electron microscopy image of (a) natural zeolite (Ze), (b) zeolite treated with HCl, (c) zeolite (Ze–Fe), (d) composite (Ze–Fe(Fe–Cu)), (e) (Ze–Fe) after contact with brilliant blue dye, and (f) composite (Ze–Fe(Fe–Cu)) after contact with brilliant blue dye, (g, h, i) TEM images of Fe–Cu nanoparticles.

observed are assigned mainly to asymmetric and symmetric stretching, which are the characteristics of this kind of materials [27]. The IR spectrum of the different zeolitic materials shows bands at 1,640 cm^{-1} corresponding to O–H vibrations of the adsorbed water molecules. The absorption band at 3,400 cm^{-1} arises from stretching vibrations of O–H and increases considerably when the zeolitic material was treated with Fe^{3+}; this change could indicate an increment of the hydroxyl groups, which means the formation of additional Brønsted acid sites. In addition, a broadening of the absorption band at 1,000–1,100 cm^{-1} was observed due to the incorporation of Fe^{3+} into the zeolite structure. Furthermore, peaks corresponding to typical frequencies of Fe–O (490, 599, 1,370, and 1,580 cm^{-1}) were not observed, probably due to the overlap of these peaks with the characteristic peaks of the zeolite [8]. Other bands corresponding to the structure of the zeolite were observed at 1,040 and 1,089–1,087 cm^{-1} related to Si–O–Si asymmetric stretching vibration, Al–O–Si, and Al–O stretching vibrations. Also, bands located in the ranges from 606 to 798 cm^{-1} and from 479 to 600 cm^{-1} are related to the stretching vibrations of zeolite framework. Peaks located at 1,500 and 2,000 cm^{-1} are from impurities which disappeared after successive acid washing (with dilute HCl) of natural zeolitic tuff [34, 35]. When a transition metal cation enters a zeolitic network by ion exchange process, only slight changes occur in the peaks located on the right side of the Si (Al)–O bands because the introduction of these cations into the zeolite structure does not cause a significant change in the zeolite network [27]. The spectra are similar to those reported in the literature [36,37], where slight changes in the bands due to the modifications and high crystallinity of the zeolite are observed.

After the contact of the material with the dye solution, a more intense vibration peak was observed at 1,065.55 cm^{-1} for Ze–Fe and 1,059.29 cm^{-1} for the composite, which can reasonably be assigned to the –Al–O– stretching

Table 1
Elemental composition of the zeolitic materials obtained by EDS

Element	% Ze	% Ze–HCl	% Ze–Fe	% Ze–Fe Saturated with dye	% Ze–Fe(Fe–Cu)	% Ze–Fe(Fe–Cu) Saturated with dye
O	47.42 ± 1.92	47.34 ± 2.27	41.50 ± 2.97	37.74 ± 2.35	34.74 ± 3.99	36.34 ± 4.18
C	–	–	–	9.67 ± 1.14	12.59 ± 0.75	26.37 ± 7.65
Na	2.79 ± 0.21	1.49 ± 0.18	0.63 ± 0.13	0.31 ± 0.05	0.54 ± 0.07	0.76 ± 0.22
Mg	0.15 ± 0.07	–	0.04 ± 0.06	–	–	0.07 ± 0.07
Al	6.74 ± 0.19	7.10 ± 0.21	5.00 ± 0.54	3.64 ± 0.45	3.32 ± 0.36	4.07 ± 0.2
Si	38.95 ± 1.52	40.30 ± 1.82	30.32 ± 2.21	21.99 ± 3.13	20.74 ± 1.97	23.37 ± 4.38
K	2.05 ± 0.23	2.18 ± 0.48	0.76 ± 0.11	0.86 ± 0.20	0.71 ± 0.10	0.82 ± 0.20
Ca	0.66 ± 0.05	0.74 ± 0.16	0.17 ± 0.05	0.26 ± 0.07	0.32 ± 0.05	0.40 ± 0.09
Cl	–	–	1.50 ± 0.33	1.45 ± 0.35	1.93 ± 0.35	0.36 ± 0.24
Fe	1.24 ± 0.48	0.86 ± 0.31	20.08 ± 4.74	24.07 ± 4.64	18.91 ± 5.37	7.19 ± 4.31
Cu	–	–	–	–	0.20 ± 0.14	0.26 ± 0.19
N	–	–	–	6.00 ± 0.29	–	–

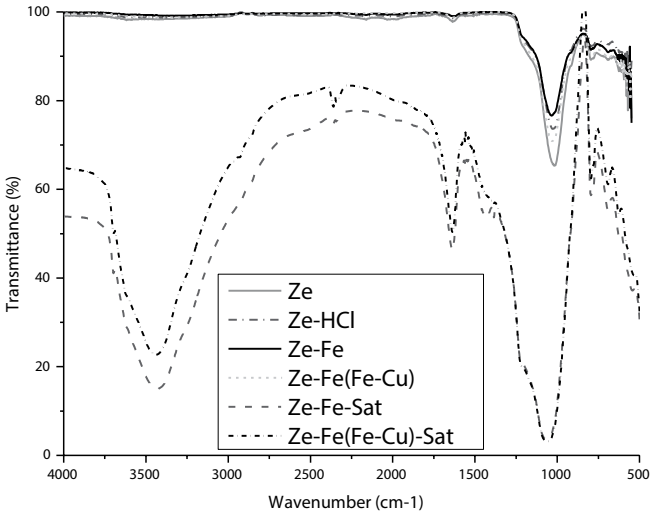

Fig. 2. IR spectrum of Ze, Ze–HCl, Ze–Fe, Ze–Fe(Fe–Cu), Ze–Fe–Sat, and Ze–Fe(Fe–Cu)–Sat.

vibrations. The band that appears at 1,600 cm^{-1} for both materials could be attributed to the vibration O–H of adsorbed zeolitic water molecules [13]. The intensive peak around 3,450 cm^{-1} for Ze–Fe and composite is assigned to the stretching of the O–H groups of the water molecules associated with Na^+ and Ca^{2+} ions contained in the zeolite channels [13]. Raman spectroscopy as a reliable technique was applied; the Raman spectra of Ze–Fe(Fe–Cu) show bands around 336, 502, and 677 cm^{-1} corresponding to γ-Fe_2O_3 and a broad band at 1,100 cm^{-1} corresponding to CuO.

3.1.3. Specific surface areas (BET)

The BET specific surface areas for the untreated, acid, Ze–Fe, and composite (Ze–Fe(Fe–Cu)) samples were 37.6, 190.1, 220.3, and 120.1 m^2/g, respectively. The specific surface area of the material treated with HCl increases because HCl removes impurities that block the pores [29]. The specific surface area increased when the sample was treated with iron chloride and decreased with the addition of nanoparticles (Fe–Cu). Doula [30] reported the presence of non-crystalline iron formations located at cationic positions in the zeolite channels, as well as the formation of iron complexes outside the cell. The specific surface areas of these materials are higher than the values reported in the literature for iron-manganese and iron-manganese-modified zeolitic tuff [23, 38].

3.1.4. Point of zero charge

Point of zero charge (pHpzc) is a concept related to adsorption phenomenon and defined as the pH at which the surface of the material is uncharged [35]. In aqueous solution, at pH higher than pHpzc, the surface is negatively charged and thus the adsorption of cations is favored. At pH lower than pHpzc, the adsorbent surface is positively charged and thus the adsorption of anions is favored [35]. The values obtained for pHpcz were 1.9 and 2 for Ze–Fe and Ze–Fe(Fe–Cu), respectively.

3.1.5. X-ray diffraction

Fig. 3 shows the diffractograms corresponding to the natural zeolite clinoptilolite-rich tuff (Ze), the Ze–Fe, and the (Ze–Fe(Fe–Cu); the diffraction patterns obtained were compared with that of clinoptilolite (JCPDS 01-089-7538) and quartz (JCPDS 03-065-0466). The diffractograms revealed the presence of clinoptilolite and mordenite; similar results have been reported in the literature for clinoptilolite-type zeolites from other natural sources [23,28,37]. These results suggest that there were not any notable change in the structure of clinoptilolite after it was treated with hydrochloric acid and iron chloride solutions, since new peaks or displacements were not observed by X-ray diffraction (XRD). The powder diffraction analysis of zeolitic tuffshowed that clinoptilolite and quartz are the main mineral phases. The mineralogical composition persisted after treatments, confirming that the conditioning mainly affects the concentrations of interchangeable ions without causing significant structural

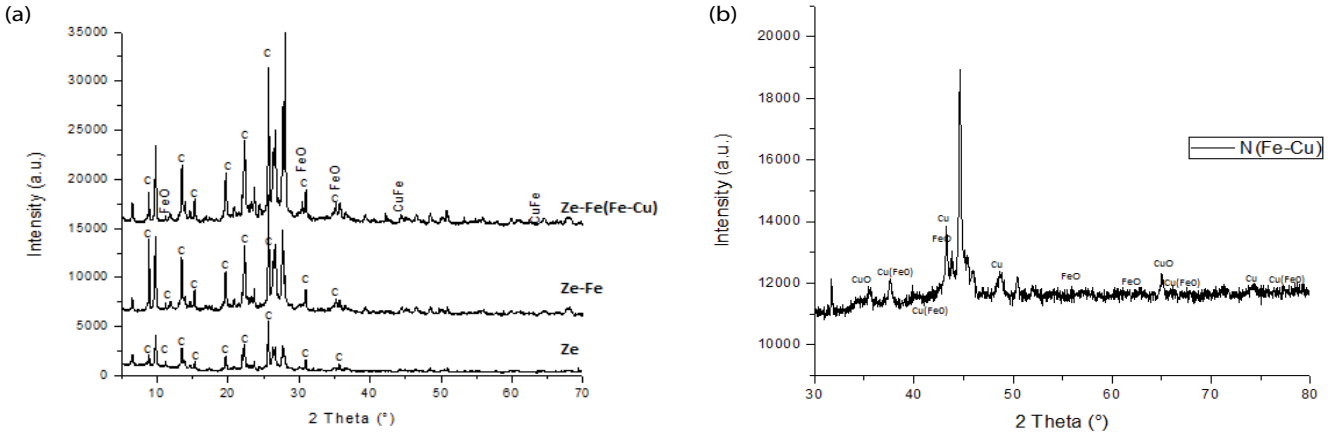

Fig. 3. XRD pattern of (a) natural zeolite (Ze), ferric zeolite (Ze–Fe), and Ze–Fe(Fe–Cu) composite (C=Clinoptilolite, FeO= Maghemite, CuFe=Copper Iron) and (b) nanoparticles N(Fe–Cu).

alterations within the tetrahedral nucleus; similar behaviors have been observed by Motsa et al. [29].

The XRD diffractograms of the zeolitic materials show characteristic peaks at 2θ of 9.876, 11.184, 13.066, 17.357, 19.099, 22.357, 22.493, 23.213, 23.817, 25.061, 25.366, 26.057, 31.361, and 36.152 which are similar to the XRD data of crystalline structure of clinoptilolite corresponding to the data [JCPDSNo.70-1859] and the literature [8,29,39]. The Ze–Fe(Fe–Cu) diffractogram indicates the presence of $Fe_{1.966}O_{2.963}$ as shown in 2θ in 11, 31, and 35 which also correspond to those reported by Nairat et al. [26]. Also the diffraction peaks at 2θ of 44.5 and 64.5 correspond to the presence of Cu_3Fe_{17} and indicate that it was deposited on the surface of the material.

The average size of the crystals was determined based on the width of XRD peak and the Bragg angle using the Scherrer equation [34,39,40]:

$$d = \frac{0.9\lambda}{\beta\cos\theta} \tag{3}$$

where d is the mean diameter of the crystal, λ the wavelength of the X-rays (Cu Ka radiation l = 1.5406 Å used), β the line of the excess width of the diffraction peak in radians, θ is the Bragg angle in grade, and k is a constant, 0.89. The mean Ze–Fe(Fe–Cu) size was estimated to be about 19.12 nm for CuO and 46.40–87.04 nm for FeO (Fig. 3(b)).

3.2. Sorption of dye

3.2.1. Sorption kinetics

Batch kinetic tests were performed to determine the times to achieve equilibrium in the adsorption systems. The dye removal kinetic results of Ze–Fe and Ze–Fe(Fe–Cu) are shown in Fig. 4. There was a significant high adsorption in the first 5 h for Ze–Fe(Fe–Cu) and 7 h for Ze–Fe, and the adsorption rate decreased up to equilibrium was reached. Equilibriums of the systems were attained in 72 h; the percent removal at equilibrium was 75.29% ± 0.90% and 87.02% ± 2.40% for Ze–Fe and Ze–Fe(Fe–Cu), respectively.

The adsorption in the first 3 h was faster; this is due to a massive diffusion of the solution to the surface of the adsorbent. Then a slower adsorption was observed until the equilibrium was reached. The speed of adsorption was faster for the Ze–Fe(Fe–Cu) composite than Ze–Fe; in addition, a greater adsorption capacity for the composite was observed (Fig. 4(a)). The adsorption capacities for Ze and Ze–HCl were lower than 0.07 and 0.1 mg/g, respectively, and then these materials were not considered for the other studies.

Zeng et al. [41] showed that the bimetallic nanocomposite system Cu–Fe exhibits higher activity for nitrate reduction achieving 100% in 6 h compared with nanoparticles. The role of Fe in the nanocomposite system Ze–Fe(Cu–Fe) is as an electron donor; the second metal Cu acts as a promoter, and thus, the reactivity increases. The presence of Cu in the bimetallic nanocomposite, at least at certain levels, can prevent iron particles from being oxidized by O_2, which can also enhance the reduction of contaminants. The results indicate that the Ze–Fe(Fe–Cu) composite has faster dye removal and larger removal capacity than Ze–Fe. This is attributed to the distribution of nano iron chains in the zeolitic tuff network, which make them kinetically more accessible for dye molecules [25]; the adsorption of dyes usually takes place in the mesopores [8]. Experimental data were fitted to the pseudo-first-order [12,42], second order [12,42,43], and pseudo-second-order [42,44] to determine the kinetic parameters of the adsorption processes. The experimental results are shown in Fig. 4; the fitting of data was performed by nonlinear regression using the program ORIGIN 8.0, and the kinetic parameters obtained are shown in Table 2.

The equations of the kinetic models are the following:
Pseudo-first-order model (Langergren):

$$q_t = q_e\left(1 - e^{k_1 t}\right) \tag{4}$$

Second-order model (Elovich):

$$q_t = \frac{1}{a}\ln\left(1 + abt\right) \tag{5}$$

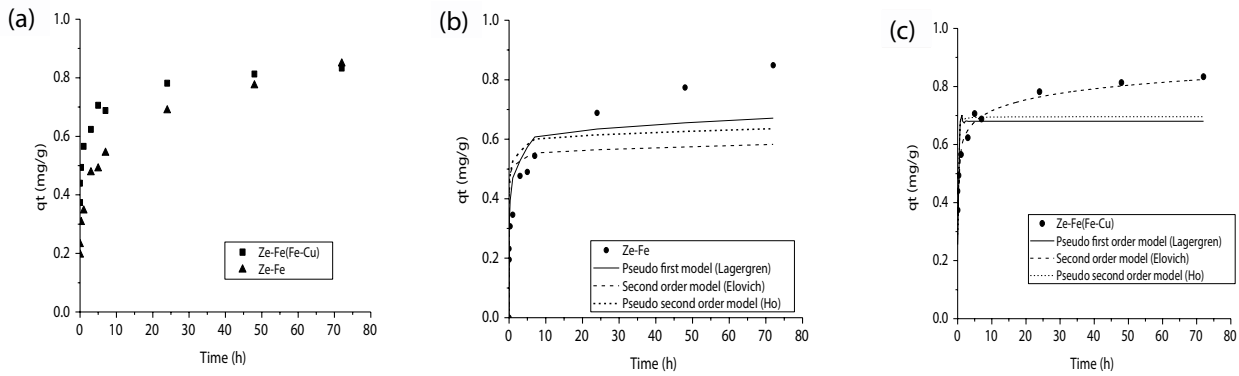

Fig. 4. (a) Sorption kinetics of brilliant blue by Ze–Fe and composite (Ze–Fe(Fe–Cu)), (b) Ze–Fe, and (c) composite (Ze–Fe(Fe–Cu)) data adjusted to kinetic models.

Table 2
Kinetic parameters of the blue brilliant adsorption by Ze–Fe and composite (Ze–Fe(Fe–Cu))

Material	Kinetic models								
	Pseudo-first-order			Second-order			Pseudo-second-order		
	q_e (mg/g)	K_L (h^{-1})	R^2	a (mg/g·h)	b (g/mg)	R^2	q_e (mg/g)	K (g/mg·h)	R^2
Ze–Fe	0.72	0.36	0.67	14.57	12.34	0.94	0.74	1.17	0.77
Ze–Fe(Fe–Cu)	0.68	31.38	0.20	2,648.78	18.28	0.94	0.69	68.14	0.42

Pseudo-second-order (Ho):

$$q_t = \frac{q_e^2 kt}{1 + q_e kt} \tag{6}$$

where k_1 (h^{-1}) is the pseudo-first-order rate constant, q_e (mg/g) and q_t (mg/g) are the adsorption capacities at the equilibrium and time t (h), respectively, a and b are the adsorption and the desorption constants, and k (g/mg·h) relates to the constant of pseudo-second-order adsorption. Data were best fitted to the second-order (Elovich) model because it shows the highest correlation coefficients (Table 2). This model has proven to be suitable for highly heterogeneous systems. The adsorption of the dye by modified clinoptilolite-rich tuff is an example of this case, since they are composed of different minerals and, therefore, have sites with different adsorption energies. The pseudo-first-order kinetic model did not have a good agreement with experimental data and has the lowest R.

3.2.2. Sorption isotherm

The equilibriums of the systems are shown in Fig. 5. It can be observed that at higher concentrations of brilliant blue, higher amounts of dye are absorbed. The adsorption isotherm models of Freundlich [45–47], Langmuir [47,48], and the Langmuir–Freundlich [49] were used to treat the adsorption data of brilliant blue by a nonlinear regression analysis using ORIGIN Pro 8.0 (for Windows). The parameters obtained by the different models are shown in Table 3.

The equations of the isotherm models are the following:

Freundlich

$$q_e = K_f C_e^{1/n} \tag{7}$$

Langmuir

$$q_e = \frac{q_0 b C_e}{1 + bC_e} \tag{8}$$

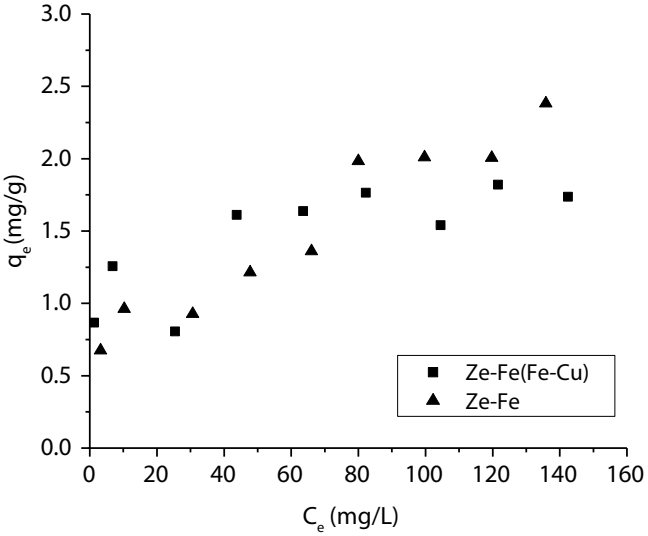

Fig. 5. Isotherms of brilliant blue adsorption by Ze–Fe and composite (Ze–Fe(Fe–Cu)).

Table 3
Langmuir, Freundlich, and Langmuir–Freundlich parameters for Ze–Fe and composite (Ze–Fe(Fe–Cu))

Material	Sorption isotherms									
	Langmuir			Freundlich			Langmuir–Freundlich			
	q_o (mg/g)	B (L/mg)	R^2	K_F (mg/L)	n	R^2	K_{LF} (L/g)	a_{LF} (mg/L)	n	R^2
Ze–Fe	3.44	0.01	0.77	0.25	2.23	0.89	Not adjusted			
Ze–Fe(Fe–Cu)	1.65	0.70	0.77	0.90	73.34	0.89	1.23	0.44	3.73	0.87

Langmuir–Freundlich

$$q_e = \frac{K_{LF} C_e^{1/n}}{1 + b_{LF} C_e^{1/n}} \tag{9}$$

where C_e is the dye concentration at equilibrium (mg/L), q_e is the adsorption capacity at equilibrium (mg/g), K_f ((mg/g) (L/g)) and K_{LF} (mg/mL), b, and $1/n$ are empirical constants related to the adsorption of dye. According to the parameters obtained from the different isotherm models, and R^2, the model that best fits the processes of adsorption of brilliant blue by both adsorbents is the Freundlich model which indicates that the adsorbent is heterogeneous. The Freundlich constant (K_f), which is proportional to the adsorption capacity, is higher for Ze–Fe(Fe–Cu) than Ze–Fe. The value of the constant $1/n$ is lower than 1 for both materials, which indicates that the adsorption is favorable. The values of n were different for both materials; the reciprocal of n showed better adsorption for the composite. This value can be compared with other works where different adsorbents are also used for water treatment; Trujillo-Reyes et al. [50] reported n = 0.477 for Fe–Ni nanostructures, 0.332 and 0.361 for C/Fe–Ni (75%/25%) and C/Fe–Ni (95%/5%) composites, respectively. Gutiérrez et al. (2009) [24] employed Ze–Fe (n = 0.66) and charcoal material from pyrolyzed sludge treated with HCl (n = 0.36). Isotherm studies of manganese removal by zeolite X and its composite materials reported by Al-Jubouri et al. [51] showed a good agreement of experimental data with Freundlich model. These results indicate heterogeneous sites on the surface of the materials. The value of $1/n < 1$ indicates high heterogeneous surface and high ion-exchange intensity at high manganese concentrations.

3.2.3. Effect of temperature

The effect of temperature on the adsorption capacity of the materials was investigated; the adsorption experiments were performed at 303, 313, and 323 K, and dye removal increased by increasing the temperature. Previous studies have also shown that adsorption capacities increase with increasing temperature, indicating the endothermic nature of the adsorption process and the favorable adsorption at higher temperature [8,52]. Temperature affects the adsorption rate by altering the molecular interactions and the solubility of the adsorbates. [29]. Thermodynamic parameters such as Gibbs free energy ($\Delta G°$), enthalpy ($\Delta H°$), and entropy ($\Delta S°$) changes play important roles in adsorption behavior; these parameters were calculated using the following equations [52–56]:

$$K_c = \frac{q_e}{C_e} \tag{10}$$

The Gibbs free energy change of the ion-exchange process was calculated by using Eq. (11):

$$\Delta G^\circ = -RT \ln K_d \tag{11}$$

Thus, the values of enthalpy ($\Delta H°$) and the entropy ($\Delta S°$) can be calculated using the van't Hoff Eq. (12)

$$\ln k_c = \frac{\Delta S^\circ}{R} - \frac{\Delta H^\circ}{RT} \tag{12}$$

where K_c (Eq. (10)) is the adsorption equilibrium constant (mL/g), R is the gas constant (8.314 KJ/mol K), T is the absolute temperature, and ΔG is the Gibbs free energy (KJ/mol). The enthalpy change $\Delta H°$ (KJ/mol) and entropy change $\Delta S°$ (KJ/mol K) were obtained by calculating the slope and intercept from plot of ln K_c versus $1/T$, and the data obtained are shown in Fig. 6 and Table 4. It can be seen that the thermodynamic equilibrium constant, K_c, increased with temperature, which indicates that sorption is an endothermic process and the values of $\Delta S°$ and $\Delta H°$ were both positive. The positive value of $\Delta S°$ suggests greater randomness at the solid/liquid interface in the sorption system and increases throughout the sorption process [56].

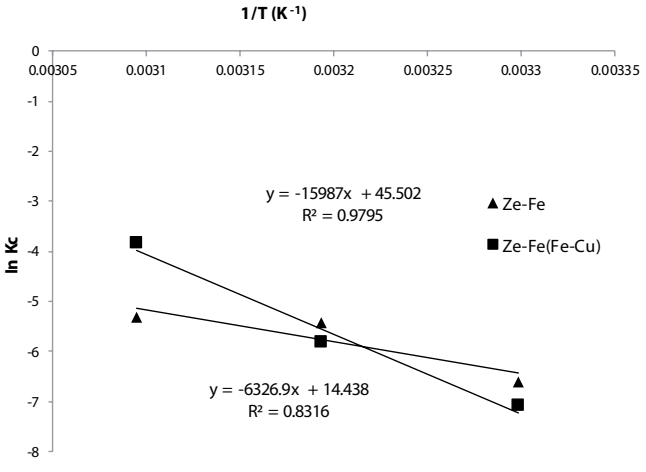

Fig. 6. lnK_c vs. $1/T$ for the adsorption of brilliant blue by Ze–Fe and Ze–Fe(Fe–Cu).

Table 4
Thermodynamic parameters of the adsorption of brilliant blue by Ze–Fe and Ze–Fe(Fe–Cu)

Material	T (K)	K_d (mL/g)	$\Delta G°$ (kJ/mol)	$\Delta H°$ (kJ/mol)	$\Delta S°$ (kJ/mol·K)
Ze–Fe	303.15	0.0009	16.62	52.60	0.12
	313.15	0.0040	14.14		
	323.15	0.0050	14.28		
Ze–Fe(Fe–Cu)	303.15	0.0007	18.15	126.29	0.3563
	313.15	0.0030	15.16		
	323.15	0.0217	10.29		

The positive value $\Delta H°$ for both materials indicated that the adsorption process is endothermic and the anions of the dyes would preferably be attached to the adsorbent materials [49]. Also, the value of $\Delta H°$ can give information about the adsorption mechanism. For the case of physical adsorption, $\Delta H°$ should be lower than 80 kJ/mol, and for chemical adsorption, it ranges between 80 and 400 kJ/mol [55]. As observed in Table 4, physical sorption process takes place for the case of Ze–Fe and chemical sorption for the case of Ze–Fe(Fe–Cu). This is because the rate of intraparticle ion diffusion increases with increasing solution temperature [51]. Positive ΔG values are observed for both materials.

3.2.4. Effect of pH

pH is one of the most important parameters in adsorption processes, especially due to its effects on the loading of the adsorbent surfaces. Experiments were conducted in the pH range 3–9. Fig. 7 shows the sorption efficiency of the brilliant blue at different pH conditions. At pH 7, the sorption capacities were q_e = 0.63 and 0.77 mg/g for Ze–Fe and Ze–Fe(Fe–Cu), respectively. The efficiencies at pH 3 were highest q_e = 0.78 mg/g (Ze–Fe) and 0.85 mg/g (Ze–Fe (Fe–Cu)) and for pH 5 = 0.62 mg/g (Ze–Fe) and 0.78 mg/g (Ze–Fe (Fe–Cu)). A similar phenomenon was observed in sorption of acid dye from aqueous solution by surfactant-modified natural zeolites where the sorption capacities decreased as the pH increased from 3 to 9 [42]. Mao et al. [57] investigated the efficiency of the degradation of soluble dyes over the pH range 5.0–9.0 by using nanoscale zero-valent iron; the dye removal efficiency increased significantly with decreasing pH. Also, Huong et al. [47] found that the pH of the solution strongly influences the adsorption process between Fe-nano zeolite and nitrophenols; in acidic conditions (pH 2–5), they achieved removal efficiencies of 95.6% for *o*-nitrophenol and 98.6% for *p*-nitrophenol. The pH affects the charge of the adsorbent surfaces and ionic forms of contaminant molecules in solution. The dye molecules appear to be protonated in acid solutions, especially between pH 3 and 5. Therefore, the force between these protonated molecules and the surface of the negatively charged adsorbents attracts the solutes to the surface of the adsorbent, resulting in a greater sorption capacity (pHpcz were 1.9 and 2 for Ze–Fe and Ze–Fe(Fe–Cu), respectively). At pH 7, one might expect that the repulsive force between the surface of the negatively charged adsorbent and the free electrons of the dye will decrease the sorption capacity; however, the

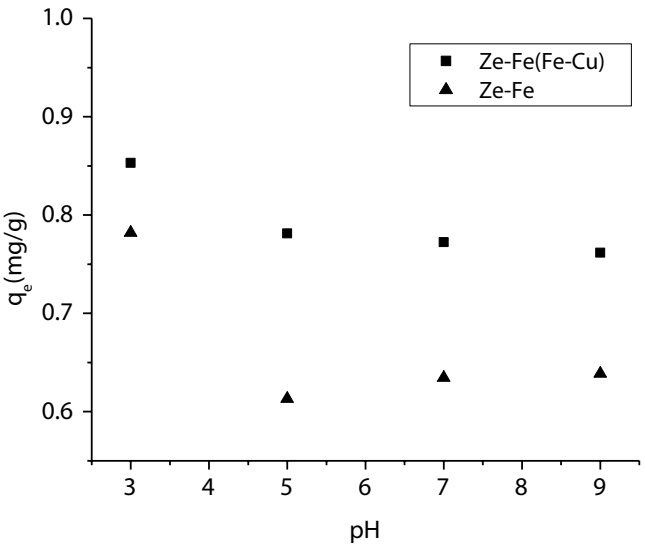

Fig. 7. pH effect on the adsorption of brilliant blue by Ze–Fe and Ze–Fe(Fe–Cu).

hydroxyl ions can interact with the dye to carry out the sorption of the dye. It is observed that from pH 7 to 9, a plateau is formed, and there is not any significant change in the sorption process.

Brilliant blue is a synthetic dye; azo type is an acid dye and contains negative sulfonic groups ($-SO_3$); the color part of the acid dye molecule is anionic. Legese et al. [18] reported that clinoptilolite as a support of nanoparticles shows a maximum color removal efficiency of 99% in acid pH.

Nezamzadeh-Ejhieh and Zabihi-Mobarakeh [58] have observed that clinoptilolite improves the reactivity of CuO when these chemical species are fixed in the ion exchange sites. The zeolite can distribute excited electrons in the CuO conductance band in its network structure, thus avoiding the recombination of electron-hole pairs. The activity of CuO–Ze depends on the effective surface of the nanoparticles. CuO in the zeolite channels can be a reason for CuO stability on the zeolite structure. The brilliant blue is an anionic dye, and therefore, it is repelled from the surface of the positively charged adsorbent at strong acidic pH values. Therefore, it is desirable to increase the pH toward pHpzc to increase the quantity of dye molecules near the surface of the material. The pollutants are adsorbed on the surface of the aluminosilicates resulting in its immobilization with the processes of coordination or ion

exchange; contaminants also can be maintained by H bonds or by Van der Waals interactions resulting from strong or weak interactions. The adsorption process is mainly electrostatic in the negative sites (the siloxane groups), forming an outer sphere complex, and a complexation in the edge sites (hydroxyl groups), forming an internal sphere complex that is mainly of chemical nature [48].

According to the BET results, the nanoparticles provide a greater surface area in the nanocomposite, compared with zeolite, and increase the capacity of zeolites in the adsorption of contaminants. This shows that most of the active adsorption sites of the nanoparticles can be found outside the adsorbent, and they are easily accessible by the contaminating ion species, resulting in higher adsorption.

4. Conclusions

The adsorption of brilliant blue by Ze–Fe(Fe–Cu) and Ze–Fe was investigated in batch system. The composite was synthesized in situ and characterized by SEM, TEM, XRD, and IR. The characterization of both materials by XRD reveals the presence of clinoptilolite and the crystallinity after the different treatments. The specific area increases from 37.67 to 220.24 m^2/g after treatments. TEM confirmed that Fe–Cu nanoparticles (11.70–15.85 nm) have been successfully loaded and efficiently dispersed on the zeolite. The adsorption was faster using Ze–Fe(Fe–Cu) composite than Ze–Fe. The removal of brilliant blue was 75.29% ± 0.90% and 87.02% ± 2.40% for Ze–Fe and Ze–Fe(Fe–Cu), respectively.

Adsorption isotherms of brilliant blue by Ze–Fe(Fe–Cu) composite and Ze–Fe showed that the Ze–Fe(Fe–Cu) composite had a higher ability than Ze–Fe for the adsorption of the dye in aqueous solution. It was observed that these materials are particularly effective on removing the dye and that the removal of dye increases when the pH decreases. The positive values of $\Delta H°$ for both materials indicated that the adsorption processes are endothermic. The results provide knowledge for the development of novel technologies using bimetallic composites to treat wastewater.

Acknowledgments

We acknowledge financial support from CONACYT, Scholarship grant 554061, for S. Pinedo-Hernández. We are thankful to Dr. Uvaldo Hernández Balderas of the powder XRD laboratory of the UAEMUNAM Joint Research Center for Sustainable Chemistry and UAEM, project 4523/2018/CI.

References

[1] A. Nezamzadeh-Ejhieh, Z. Banan, Sunlight assisted photodecolorization of crystal violet catalyzed by CdS nanoparticles embedded on zeolite A, Desalination, 284 (2012) 157–166.
[2] R. Aravindhan, N.N. Fathima, J.R. Rao, B.U. Nair, Wet oxidation of acid brown dye by hydrogen peroxide using heterogeneous catalyst Mn-salen-Y zeolite: a potential catalyst, J. Hazard. Mater., 138 (2006) 152–159.
[3] M. Flury, H. Flühler, Tracer characteristics of brilliant blue FCF, Soil Sci. Soc. Am. J., 59 (1995) 22–27.
[4] A. Mittal, Use of hen feathers as potential adsorbent for the removal of a hazardous dye, Brilliant Blue FCF, from wastewater, J. Hazard. Mater., 128 (2006) 233–239.
[5] Y. Ni, Y. Wang, S. Kokot, Simultaneous kinetic spectrophotometric analysis of five synthetic food colorants with the aid of chemometrics, Talanta, 78 (2009) 432–441.
[6] EPA, Inert Reassessment Document for FD&C Blue No. 1, EPA (Environmental Protection Agency).
[7] C. Morris, S.J. Mooney, S.D. Young, Sorption and desorption characteristics of the dye tracer, Brilliant Blue FCF, in sandy and clay soils, Geoderma, 146 (2008) 434–438.
[8] M. Akgül, Enhancement of the anionic dye adsorption capacity of clinoptilolite by Fe^{3+}-grafting, J. Hazard. Mater., 267 (2014) 1–8.
[9] Q. Chen, P. Wu, Z. Dang, N. Zhu, P. Li, J. Wu, X. Wang, Iron pillared vermiculite as a heterogeneous photo-Fenton catalyst for photocatalytic degradation of azo dye reactive brilliant orange X-GN, Sep. Purif. Technol., 71 (2010) 315–323.
[10] N. Arabpour, A. Nezamzadeh-Ejhieh, Modification of clinoptilolite nano particles with iron oxide: increased composite catalytic activity for photodegradation of cotrimaxazole in aqueous suspension, Mater. Sci. Semicond. Process., 31 (2015) 684–692.
[11] V.K. Gupta, S. Suhas, Application of low-cost adsorbents for dye removal: a review, J. Environ. Manage., 90 (2009) 2313–2342.
[12] E. Zanin, J. Scapinello, M. De Oliveira, C. Rambo, F. Franscescon, L. Freitas, J.M. Muneron de Mello, M.A. Fiori, J. Vladimir de Oliveira, J. Dal Magro, Adsorption of heavy metals from wastewater graphic industry using clinoptilolite zeolite as adsorbent, Process Saf. Environ. Prot., 105 (2016) 194–200.
[13] A. Nezamzadeh-Ejhieh, S. Moeinirad, Heterogeneous photocatalytic degradation of furfural using NiS-clinoptilolite zeolite, Desalination, 273 (2011) 248–257.
[14] B. Armagan, O. Ozdemir, M. Turan, M.S. Celik, The removal of reactive azo dyes by natural and modified zeolites, J. Chem. Technol. Biotechnol., 78 (2003) 725–732.
[15] S. Haji, M. Khalaf., M. Shukrallah, J. Abdullah, S. Ahmed, A kinetic comparative study of azo dye decolorization by catalytic wet peroxide oxidation using Fe–Y zeolite/H_2O_2 and photooxidation using UV/H_2O_2, React. Kinet. Mech. Catal., 114 (2015) 795–815.
[16] B. Dutta, S. Jana, A. Bhattacharjee, P. Gütlich, I. Sei-Ichiro, S. Koner, c-Fe_2O_3 nanoparticle in NaY-zeolite matrix: preparation, characterization, and heterogeneous catalytic epoxidation of olefins, Inorg. Chim. Acta, 363 (2010) 696–704.
[17] T. Shahwan, S.A. Sirriah, M. Nairat, E. Boyaci, A.E. Eroğlu, T.B. Scott, K.R. Hallam, Green synthesis of iron nanoparticles and their application as a Fenton-like catalyst for the degradation of aqueous cationic and anionic dyes, Chem. Eng. J., 172 (2011) 258–266.
[18] H.S. Legese, N.B. Unni, M. Redi-Abshiro, R. Aravindhan, I. Diaz, M. Tessema, Synthesis, characterization and catalytic application of zeolite based heterogeneous catalyst of iron(III), nickel(II) and copper(II) salen complexes for oxidation of organic pollutants, J. Porous Mater., 22 (2015) 1363–1373.
[19] V.S. Radomskii, E.S. Astapova, S.M. Radomskii, Structure and thermal properties of zeolites modified with Fe and Cu nanopowders, Inorg. Mater., 51 (2015) 999–1007.
[20] L. Sun, H. Song, Q. Li, A. Li, Fe/Cu bimetallic catalysis for reductive degradation of nitrobenzene under oxic conditions, Chem. Eng. J., 283 (2016) 366–374.
[21] Y. Ren, Y. Yuan, B. Lai, Y. Zhou, J. Wang, Treatment of reverse osmosis (RO) concentrate by the combined Fe/Cu/air and Fenton process (1st Fe/Cu/air-Fenton-2nd Fe/Cu/air), J. Hazard. Mater., 302 (2016) 36–44.
[22] R. Pérez, M.P. Elizalde, U. Bentrup, Preparation and in situ spectroscopic characterization of Cu-clinoptilolite catalysts for the oxidative carbonylation of methanol, Microporous Mesoporous Mater., 164 (2012) 93–98.
[23] E. Gutiérrez, M. Solache-Ríos, A. Colin, Sorption of indigo carmine by a Fe-zeolitic tuff and carbonaceous material from pyrolyzed sewage sludge, J. Hazard. Mater., 170 (2009) 1227–1235.
[24] M. Solache-Ríos, R. Villalva-Coyote, M.C. Díaz-Nava, Sorption and desorption of remazol yellow by a Fe-zeolitic tuff, J. Mex. Chem. Soc., 54 (2010) 58–66.
[25] M. Nairat, T. Shahwan, A.E. Eroğlu, H. Fuchs, Incorporation of iron nanoparticles into clinoptilolite and its application for the removal of cationic and anionic dyes, J. Ind. Eng. Chem., 21 (2015) 1143–1151.

[26] F.A. Mumpton, O.W. Clayton, Morphology of zeolites in sedimentary rocks by scanning electron microscopy, Clays Clay Miner., 24 (1976) 1–23.
[27] D.W. Breck, Zeolite Molecular Sieves, John Wiley & Sons, New York, 1974.
[28] G. Tsitsishvilli, T. Andronikashuili, G. Kirov, L.D. Filizova, Natural Zeolites, Ellis Horwood Limited, Chichester, England, 1992.
[29] M.M. Motsa, B.B. Mambaa, J.M. Thwala, T.A.M. Msagati, Preparation, characterization, and application of polypropylene–clinoptilolite composites for the selective adsorption of lead from aqueous media, J. Colloid Interface Sci., 359 (2011) 210–219.
[30] M. Doula, Synthesis of a clinoptilolite–Fe system with high Cu sorption capacity, Chemosphere, 67 (2007) 731–740.
[31] E. Xingu-Contreras, G. García-Rosales, A. Cabral-Prieto, I. García-Sosa, Degradation of methyl orange using iron boride nanoparticles supported in a natural zeolite, Environ. Nanotechnol. Monit. Manage., 7 (2016) 121–129.
[32] M. Trgo, J. Perić, Interaction of the zeolitic tuff with Zn-containing simulated pollutant solutions, J. Colloid Interface Sci., 260 (2003) 166–175.
[33] S. Pinedo-Hernández, C. Díaz-Nava, M. Solache-Ríos, Sorption behavior of brilliant blue FCF by a Fe-zeolitic tuff, Water Air Soil Pollut., 223 (2012) 467–475.
[34] M. Bahrami, A. Nezamzadeh-Ejhieh, Effect of supporting and hybridizing of FeO and ZnO semiconductors onto an Iranian clinoptilolite nano-particles and the effect of ZnO/FeO ratio in the solar photodegradation of fish ponds waste water, Mater. Sci. Semicond. Process., 27 (2014) 833–840.
[35] H. Zabihi-Mobarakeh, A. Nezamzadeh-Ejhieh, Application of supported TiO_2 onto Iranian clinoptilolite nanoparticles in the photodegradation of mixture of aniline and 2, 4-dinitroaniline aqueous solution, J. Ind. Eng. Chem., 26 (2015) 315–321.
[36] E. Gutiérrez-Segura, M. Solache-Ríos, A. Colín-Cruz, C. Fall, Adsorption of cadmium by Na and Fe modified zeolitic tuffs and carbonaceous material from pyrolyzed sewage sludge, J. Environ. Manage., 97 (2012) 6–13.
[37] A. de J. Montes-Luna, N.C. Fuentes-López, Y.A. Perera-Mercado, O. Pérez-Camacho, G. Castruita-de León, S.P. García-Rodríguez, M. García-Zamora, Caracterización de clinoptilolita natural y modificada con Ca^{2+} por distintos métodos físico-químicos para su posible aplicación en procesos de separación de gases, Superficies Vacío, 28 (2015) 5–11.
[38] M.J. Jimenez-Cedillo, M.T. Olguin, C. Fall, Adsorption kinetic of arsenates as water pollutant on iron, manganese and iron–manganese-modified clinoptilolite-rich tuffs, J. Hazard. Mater, 163 (2009) 939–945.
[39] S. Sharafzadeh, A. Nezamzadeh-Ejhieh, Using of anionic adsorption property of a surfactant modified clinoptilolite nano-particles in modification of carbon paste electrode as effective ingredient for determination of anionic ascorbic acid species in presence of cationic dopamine species, Electrochim. Acta, 184 (2015) 371–380.
[40] S. Jafari, A. Nezamzadeh-Ejhieh, Supporting of coupled silver halides onto clinoptilolite nanoparticles as simple method for increasing their photocatalytic activity in heterogeneous photodegradation of mixture of 4-methoxy aniline and 4-chloro-3-nitro aniline, J. Colloid Interface Sci., 490 (2017) 478–487.
[41] Y. Zeng, H. Walker, Q. Zhu, Reduction of nitrate by NaY zeolite supported Fe, Cu/Fe and Mn/Fe nanoparticles, J. Hazard. Mater., 324-B (2016) 605–616.
[42] N. Mirzaei, M. Hadib, M. Gholamic, R.F. Fardd, M.S. Aminabad, Sorption of acid dye by surfactant modificated natural zeolites, J. Taiwan Inst. Chem. Eng., 59 (2016) 186–194.
[43] Y.S. Ho, Using of pseudo-second-order model in adsorption, Environ. Sci. Pollut. Res., 21 (2014) 7234–7235.
[44] Y.S. Ho, Review of second-order models for adsorption systems, J. Hazard. Mater., 136 B (2006) 681–689.
[45] V.V. Panic, S.J. Velickovic, Removal of model cationic dye by adsorption onto poly(methacrylic acid)/zeolite hydrogel composites: kinetics, equilibrium study and image analysis, Sep. Purif. Technol., 122 (2014) 384–394.
[46] L. Lin, Y. Lin, C. Li, D. Wu, K. Deyi, H. Kong, Synthesis of zeolite/hydrous metal oxide composites from coal fly ash as efficient adsorbents for removal of methylene blue from water, Int. J. Miner. Process, 148 (2016) 32–40.
[47] P. Huong, B. Lee, J. Kim, C. Lee, Nitrophenols removal from aqueous medium using Fe-nano mesoporous zeolite, Mater. Des., 101 (2016) 210–217.
[48] K. Kalantari, Rapid and high capacity adsorption of heavy metals by Fe_3O_4/montmorillonite nanocomposite using response surface methodology: Preparation, characterization, optimization, equilibrium isotherms, and adsorption kinetics study, J. Taiwan Inst. Chem. Eng., 49 (2015) 192–198.
[49] A.O. Moamen, H.A. Ibrahim, N. Abdelmonem, I.M. Ismail, Thermodynamic analysis for the sorptive removal of cesium and strontium ions onto synthesized magnetic nano zeolite, Microporous Mesoporous Mater., 223 (2016) 187–195.
[50] J. Trujillo-Reyes, M. Solache-Ríos, A.R. Vilchis-Nestor, V. Sánchez-Mendieta, A. Colín-Cruz, Fe–Ni Nanostructures and C/Fe–Ni composites as adsorbents for the removal of a textile dye from aqueous solution, Water Air Soil Pollut., 223 (2012) 1331–1341.
[51] S.M. Al-Jubouri, S.M. Holmes, Hierarchically porous zeolite X composites for manganese ion-exchange and solidification: equilibrium isotherms, kinetic and thermodynamic studies, Chem. Eng. J., 308 (2017) 476–491.
[52] Y. Huang, W. Wang, Q. Feng, F. Dong, Preparation of magnetic clinoptilolite/$CoFe_2O_4$ composites for removal of Sr^{2+} from aqueous solutions: Kinetic, equilibrium, and thermodynamic studies, J. Saudi Chem. Soc., 21 (2017) 58–66.
[53] M. Akhtar, S.M. Hasany, M.I. Bhanger, S. Iqbal, Low cost sorbents for the removal of methyl parathion pesticide from aqueous solutions, Chemosphere, 66 (2007) 1829–1838.
[54] Z. Cao, Y. Yue, H. Zhong, P. Qiu, P. Chen, X. Wen, S. Wang, The cationic dye removal by novel Si-Zn composites prepared from zinc ash, J. Taiwan Inst. Chem. Eng., 71 (2016) 464–473.
[55] M. Ghasemi, H. Javadian, N. Ghasemi, S. Agarwal, V.K. Gupta, Microporous nanocrystalline NaA zeolite prepared by microwave assisted hydrothermal method and determination of kinetic, isotherm and thermodynamic parameters of the batch sorption of Ni (II), J. Mol. Liq., 215 (2016) 161–169.
[56] E. Fosso-Kankeu, H. Mittal, F. Waanders, S.S. Ray, Thermodynamic properties and adsorption behavior of hydrogel nanocomposites for cadmium removal from mine effluents, J. Ind. Eng. Chem., 48 (2017) 151–161.
[57] Y. Mao, Z. Xi, W. Wang, C. Ma, Q. Yue, Kinetics of Solvent Blue and Reactive Yellow removal using microwave radiation in combination with nanoscale zero-valent iron, J. Environ. Sci., 30 (2015) 164–172.
[58] A. Nezamzadeh-Ejhieh, H. Zabihi-Mobarakeh, Heterogeneous photodecolorization of mixture of methylene blue and bromophenol blue using CuO-nano-clinoptilolite, J. Ind. Eng. Chem., 20 (2014) 1421–1431.